RSC Advances

PAPER

View Article Online
View Journal | View Issue

Cite this: *RSC Adv.*, 2020, **10**, 36349

Immobilizing a visible light-responsive photocatalyst on a recyclable polymeric composite for floating and suspended applications in water treatment†

Ch. Tahir Mehmood,[a] Ziyi Zhong,[b] Hua Zhou,[c] Chenchen Zhang[b] and Yeyuan Xiao *[a]

A visible light responsive TiO_2/Ag_3PO_4 (10 : 1) nanocomposite was prepared and successfully immobilized (12 wt%) in a spherical polymeric matrix consisting of polysulfone and alginate (10 : 6). The resulted beads featured a sponge-like structure with interconnected macrovoids and micropores, and showed high adsorption and visible-light photocatalytic activity towards various wastewater pollutants, including the widely used dye – methylene blue ($k = 0.0321\ min^{-1}$), and two emerging pharmaceutical contaminants – diclofenac ($k = 0.018\ min^{-1}$) and triclosan ($k = 0.052\ min^{-1}$). As determined, the $^{\bullet}OH$ radical and h^+ are the primary reactive oxygen species responsible for the photodegradation. The composite photocatalytic beads are also effective in bacterial inactivation and degradation of acyl-homoserine lactones (AHLs), the bacterial quorum sensing autoinducers triggering biofilms, thus exhibiting a promising future in wastewater disinfection and biofilm retardation. Additionally, these beads could be used in inter-switchable suspended or buoyant forms, and be effectively regenerated by H_2O_2 treatment, and used for multiple cycles without any significant loss in photoactivity. With these unique features, the prepared visible-light photocatalytic beads could be easily applied in large-scale water and wastewater treatment systems.

Received 9th August 2020
Accepted 22nd September 2020

DOI: 10.1039/d0ra06864k

rsc.li/rsc-advances

1. Introduction

The TiO_2-based nanomaterials are still the most economical and efficient photocatalysts to degrade various water pollutants,[1,2] despite the efforts in searching for other metal oxides over the last few decades. TiO_2 displays higher photoactivity than other semiconductors under UV irradiation, but its wide bandgap prevents the utilization of photons in the visible region. In contrast, photocatalysts with narrow bandgaps can utilize visible light, although their stability needs improvement.[3] Coupling TiO_2 with narrow-bandgap semiconductors can extend the photo-response region to visible light and enhance the separation of photoinduced charges by forming well-matched heterogeneous junctions.

Ag_3PO_4, with a narrow bandgap, is a potential candidate to separate the electron–hole pairs of TiO_2 efficiently to improve photocatalysis. Ag_3PO_4 has been considered as an extremely promising auxiliary material for constructing visible light photocatalysts by forming heterojunction.[4,5] However, the efficiency of Ag_3PO_4 decreases quickly after the initial use, due to the inherent fast charge recombination and its self-reduction to silver during photocatalysis.[6] The widely agreed strategy is to couple Ag_3PO_4 with other semiconductors such as AgCl, $In(OH)_3$, SnO_2, Bi_2WO_6, CeO_2, and other materials like graphene, PAN, *etc.*, to improve its photoactivity and stability.[7] The composite of Ag_3PO_4/TiO_2 photocatalyst has also been widely investigated and proved to be significantly better in photodegradation of various pollutants under visible light than the Ag_3PO_4 itself.[4,8,9]

While significant progress has been made on increasing the visible light-harvesting efficiency of various photocatalysts, recovery and regeneration of them in large-scale applications remain a big challenge. Immobilization of photocatalysts in appropriate adsorptive material will facilitate the easy recovery of catalysts[10,11] and enhance photodegradation *via* bringing the pollutants near the active sites of catalysts. Moreover, buoyant immobilization material is highly desirable for applications with sunlight as the irradiation source.[3,12–14] Therefore, novel supporting materials with intensified adhesion of catalysts, super adsorption capacity, and controllable interconversion

[a]*Department of Civil and Environmental Engineering, College of Engineering, Shantou University, Shantou, Guangdong, 515063, China. E-mail: yeyuanxiao@stu.edu.cn*
[b]*Department of Chemical Engineering, Guangdong Technion – Israel Institute of Technology, Shantou, Guangdong, 515063, China*
[c]*Guangdong Guangye Environmental Protection Industrial Group Co., Ltd., Guangzhou, Guangdong, China*

† Electronic supplementary information (ESI) available. See DOI: 10.1039/d0ra06864k

between buoyancy and suspension are needed for versatile applications of photocatalysis.

In our recent study, polysulfone (PSF) and alginate (Alg) were used together to immobilize TiO_2 nanoparticles in macro beads (o.d. $\sim$ 3 mm), which showed a high photocatalytic activity under UV irradiation, thermal stability, long-term durability, and facile interconversion between buoyancy and suspension. The objective of this study was to develop immobilized visible light-responsive photocatalysts further. To this end, Ag_3PO_4 was immobilized together with TiO_2 in the PSF/Alg beads. The photocatalytic efficiency of these beads was further enhanced by improving the pore architecture and modifying the surface with the post-treatment. Performance and reusability of these beads for water purification were assessed using a dye methylene blue (MB) and two emerging pharmaceuticals (diclofenac and triclosan) as the target pollutants. The photocatalytic degradation mechanism was further examined with the reactive oxygen species (ROS) scavenging experiments. In addition, bacterial inactivation and degradation of acyl-homoserine lactones (AHLs), a type of bacterial signalling molecules promoting biofilm formation, were examined to evaluate its application for water disinfection and biofilm mitigation.

2. Experimental

2.1. Material

Granular PSF, sodium alginate (SA), *N*-methyl-2-pyrrolidone (NMP) with a purity of 99%, methylene blue (MB), diclofenac (DCF), triclosan (TCS), AHLs, and titanium tetra isopropoxide (TTIP) were obtained from local suppliers. Ultrapure (UP) water obtained from an OLABO system ($\geq$18.2 MΩ-cm) was used in all experiments. Other analytical grade chemicals like sodium hydroxide, hydrochloric acid, calcium chloride, sulfuric acid, sodium nitrate, silver sulphate, polyethylene glycol (PEG8000), and ethyl alcohol were purchased from Aladdin Industrial Corporation (Shanghai, China) and used without any further purification or pre-treatment.

2.2. Preparation of TiO_2/Ag_3PO_4 photocatalyst

TiO_2 nanoparticles were prepared by a sol–gel method using TTIP as a precursor. The TiO_2/Ag_3PO_4 photocatalyst was prepared using a simple precipitation method. Typically, a certain amount of the as-prepared TiO_2 was added to a flask containing 100 mL of 1% PEG-8000 dissolved in UP water and stirred for 30 minutes, and 50 mL of Na_2HPO_4 (0.1 mol L^{-1}) aqueous solution was added and stirred for additional 10 minutes. Then, under vigorous stirring, 50 mL of $AgNO_3$ (0.3 mol L^{-1}) was added dropwise with a peristaltic pump at room temperature. After 3 h stirring, the yellow precipitate was allowed to settle for 12 h, filtered, washed, dried at 105 °C, and calcined at 400 °C for 4 h. The resulting TiO_2/Ag_3PO_4 photocatalyst was stored in the dark prior to characterization and photocatalytic reactions. For comparison, Ag_3PO_4 was prepared under the same condition without the addition of TiO_2 nanoparticles.

2.3. Preparation of polymer beads and immobilization of TiO_2/Ag_3PO_4

To prepare the PSF/Alg beads, the desired amount (2, 4, 6, 8, 10%) of Alg was added slowly to a PSF (10% w/v) solution in NMP under vigorous stirring; then the mixture was dripped into a 4% (w/v) $CaCl_2$ solution through a nozzle to form spherical beads with o.d. of $\sim$3 mm. The beads were gently stirred for 24 h to guarantee complete phase inversion, and then washed and stored separately prior to use. The adsorption capacity of the PSF/Alg beads was evaluated with MB, and the beads with 6% Alg (PA6) were selected as the immobilization material. TiO_2/Ag_3PO_4 nanoparticles were added (12% w/v) to the PSF/Alg solution prior to dripping into the $CaCl_2$ solution to form PSF/Alg/TiO_2/Ag_3PO_4 (PATAg) composite beads. For surface modification, the photocatalytic PATAg beads were gently stirred in acetone and NMP for a couple of minutes, respectively, and then sequentially rinsed with acetone, ethanol and UP water. The resulting beads were stored in a mild $AgNO_3$ solution under dark.

2.4. Conversion of PATAg beads between floating and suspended forms

Controlled interconversion of the PATAg beads between suspended and floating forms was realized with a simple drying and wetting method. The water inside the beads could be removed by drying at 50 °C for 1 h and added back again by boiling the beads for one minute and placing them in cold water, which resulted in buoyant and suspended beads, respectively.

2.5. Characterization of materials

The beads and photocatalysts were characterized by X-ray diffraction (XRD), field emission scanning electron microscope (FE-SEM), Brunauer, Emmett and Teller (BET) adsorption analyzer, thermogravimetric analyzer (TGA), and attenuated total reflection Fourier transform infrared spectroscopy (ATR-FTIR). The surface roughness of the PATAg beads was measured using a scanning probe microscope (SPM). Detailed methods are provided in ESI (Text S1).†

2.6. Adsorption experiments

Adsorption capacities of the beads were investigated using MB solution (3.2 mg L^{-1}), which was added to a 15 mL quartz vial (effective volume of 10 mL) together with 0.5 g (approx. 50 beads) of the adsorbent and shaken at 150 rpm under darkness. The MB concentration was measured at a specific time interval using a UV-visible spectrophotometer (Lambda 950, PerkinElmer) at 664 nm.

2.7. Photocatalytic degradation experiments

Photocatalytic activity of the prepared powdered photocatalysts and photocatalytic beads in suspended and buoyant (only for the PATAg beads) form was first determined using MB as the target pollutant. Two pharmaceutically active compounds (PhACs), *i.e.*, diclofenac, an anti-inflammatory drug, and triclosan, a broad-spectrum antibiotic, both have been widely

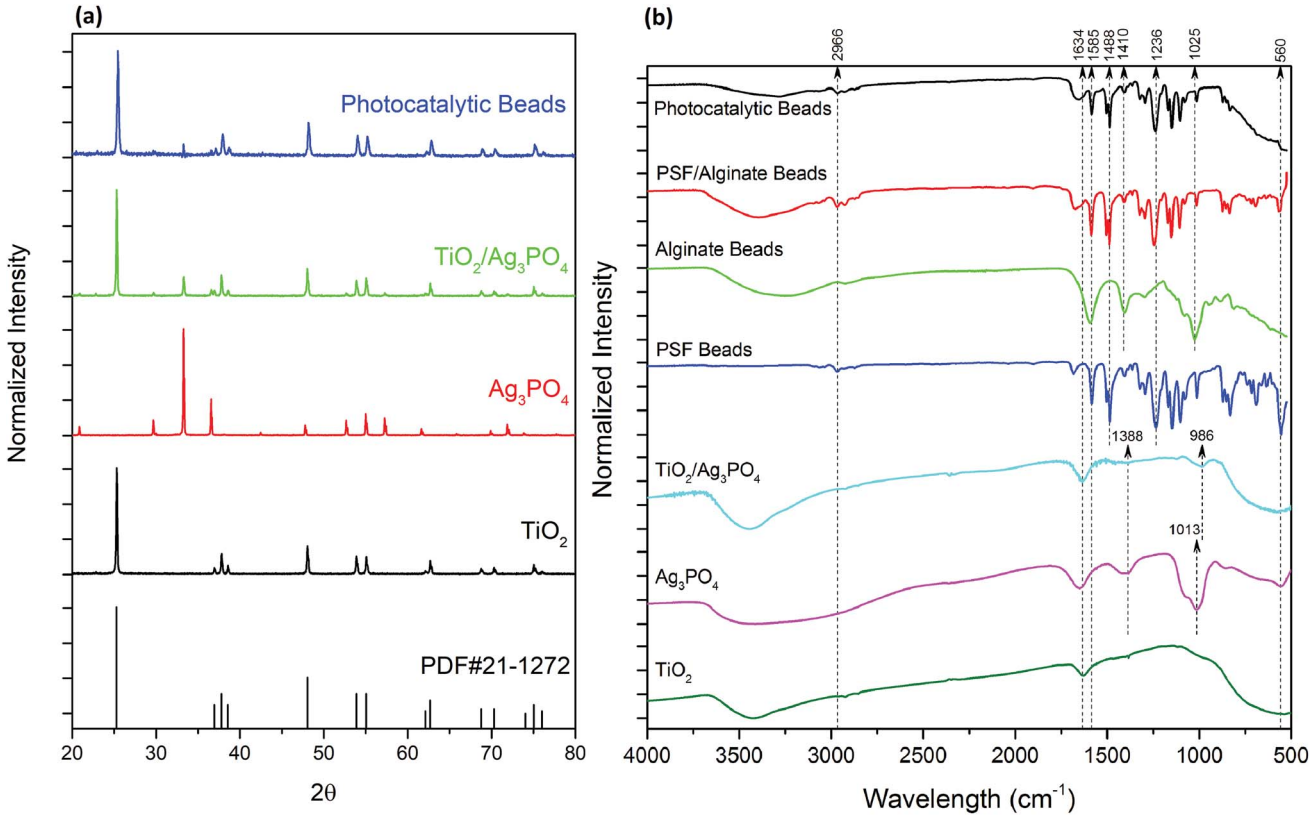

Fig. 1 XRD patterns (a) and ATR-FTIR spectrum (b) of photocatalytic powders and beads.

detected in aquatic environments, were selected as the target emerging contaminants further to evaluate the broad application potential of the PATAg beads.

2.7.1. Batch degradation in suspended form. All batch photocatalytic experiments were carried out in a 0.8 L laboratory-scale photocatalytic reactor equipped with a 15 W UV (Philips UV lamp, with an emission λ_{max} at 254 nm) or 15 W tubular LED light. The powdered catalysts (50 mg L^{-1}) were maintained in suspension *via* sparging air at a flow rate of 1.5 L min^{-1}. Before exposure to light, sparging was on for 30 min under darkness to reach adsorption/desorption equilibrium. The effects of beads dose (5, 10, 15 g L^{-1}), initial MB concentration (1.6, 3.2, 6.4 mg L^{-1}), pH (3, 7, 10) and background ions (tap water, Table S1†) were examined. To evaluate the durability of the PATAg beads, we carried out the cyclic tests under the same condition, and the beads were washed and regenerated after each cycle.

Photocatalytic degradation of diclofenac and triclosan was evaluated using the same setup with an initial PhAC concentration of 20 mg L^{-1}. The concentrations of diclofenac and triclosan in filtered samples (0.22 μm) were monitored using a UV-vis spectrophotometer at 275 and 280 nm, respectively.

2.7.2. Photocatalytic degradation of MB in floating form. Photodegradation of MB *via* the buoyant beads was carried out in a flat-bed photoreactor with an 0.8 L working volume, baffled and equipped with 3 air spargers. An overhead 200 W LED light was placed 15 cm above the water surface. Air was sparged at 0.5 L min^{-1} to provide the oxygen required for the photooxidation process. The flat-bed photoreactor was operated at batch mode with continuous effluent recirculation during the operation.

2.7.3. Regeneration of photocatalytic beads. A very simple yet effective method was employed to regenerate the PATAg beads based on an earlier report[15] with some modifications. Typically, 5 g of used photocatalytic beads were added to 60 mL UP water containing 1 mL H_2O_2 (30%) and stirred for 5 minutes; the beads were then washed with UP water for several times and

Table 1 FTIR peak assignments

Material	Peaks	Characteristic bands
Polysulfone	1148	O=S=O stretching (symmetric)
	1293	O=S=O stretching (asymmetric)
	2800–3000	Aliphatic and aromatic groups
	1236	C–O–C stretching (asymmetric)
	1488	Benzene (semi-ring stretch)
	1585	Benzene ring (quadrant stretch)
Alginate	3000–3600	O–H functional group
	1025	–C–O groups
TiO_2	500–900	Ti–O stretching
Ag_3PO_4	3400	–OH stretching
	1650	–OH vibration
	1388	P=O stretching vibration
	1013	P–O–P stretching vibrations
	560	O=P–O bending vibration

employed for next use. Compared to the earlier report,[15] this method consumes a lower concentration of H_2O_2 (1 mL in 60 mL *vs.* 1.8 mL in 60 mL), takes a much shorter period of time (5 min *vs.* 5 h), and is exempt from the need for extended drying (12 h at 65 °C).

2.7.4. Scavenger experiments for reactive oxygen species (ROS). To reveal the photodegradation mechanism of MB, we added ROS scavengers of ammonium oxalate (AO), 1,4-benzoquinone (*p*-BQ), and methanol (MeOH) separately to the MB solution during photodegradation. A borosilicate Petri plate was used as the photoreactor; 10 mM of a specific scavenger and the PATAg beads (100 ± 5) were added consecutively to 50 mL of a MB solution (6.4 mg L^{-1}) pre-sparged with air for 15 minutes. Then the reactor was illuminated with a 200 W LED lamp. Samples were taken at pre-set intervals and the MB concentration analyzed.

2.8. Bacterial disinfection and AHLs degradation

The utilization of these beads for bacterial disinfection and quorum quenching (AHLs degradation) was also assessed. The overnight-culture of a bacterial strain (*Pseudomonas fluorescens*), maintained in the LB broth, was used to evaluate the capability of the PATAg beads for bacterial inactivation. The PATAg beads (50 ± 3) were dispersed in 50 mL of PBS solution containing bacterial strain, and then illuminated with a 200 W LED lamps for a certain time. Samples were taken regularly, and 100 μL of 10-fold serially diluted samples were spread on LB Agar plates and incubated at 37 °C for 24 h; the colony-forming units (CFUs) were determined as the bacterial content in each sample. All experiments were repeated three times, and the average values were presented.

AHLs are crucial quorum sensing autoinducers for biofilm formation. Quorum Quenching (QQ), which reduces or depletes the AHL levels *via* microbial or enzymatic measures, has been used for biofouling control in wastewater treatment membrane bioreactors; however, utilization in the field is difficult or too costly.[16] Hence, use of the PATAg beads as an alternative QQ technology was evaluated. Fifty milliliters (50 mL) of 6-AHLs mixture (0.5 mM each) were placed in a borosilicate Petri plate;

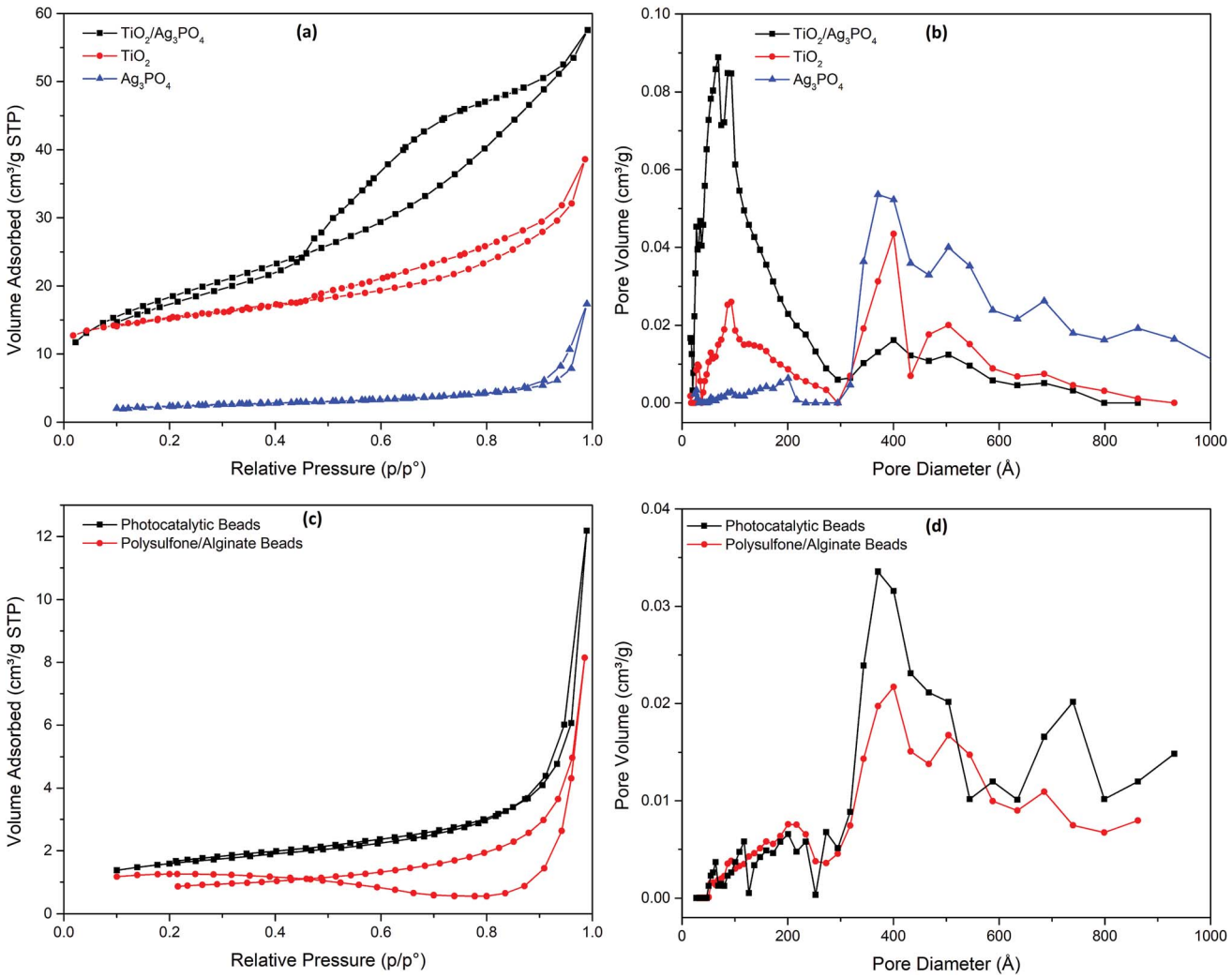

Fig. 2 Nitrogen adsorption–desorption isotherms and pore size distribution curves of (a and b) photocatalyst powders and (c and d) polymer (PSF/Alg) and photocatalytic (PATAg) beads.

50 PATAg beads were added and exposed to visible light (200 W LED lamp) for a certain time. Samples were taken and filtered through 0.22 μm syringe filters; the AHL concentration was determined by a LC/MS/MS (LCMS-TSQ-Endura, Thermo Fisher, China).

3. Results and discussion

3.1. Characterization of materials

The XRD patterns of the prepared photocatalysts are shown in Fig. 1a. All diffraction peaks of pure TiO_2 could be indexed to the anatase phase of TiO_2, according to PDF card no. 21-1272, which shows peaks at 25.3°, 36.9°, 37.8°, 38.6°, 48.0°. The XRD pattern of Ag_3PO_4 is in good agreement with the standard Ag_3PO_4 (JCPDS no. 06-0505), and the dominant peaks at 33.3° and 36.6° correspond to the (2 1 0) and (2 1 1) planes, respectively. All the peaks that appeared in pure TiO_2 were also found in the TiO_2/Ag_3PO_4 composite indicating the stability of the TiO_2 crystallinity. In contrast, the intensity of diffraction peaks for Ag_3PO_4 was significantly reduced owing to its lower concentration.

ATR-FTIR was used for the evaluation of functional groups (Fig. 1b). The absorbance peaks of the TiO_2 sample between 900 and 500 cm^{-1} could be assigned to the Ti–O stretching bands, which agrees with XRD results for rutile TiO_2. Ag_3PO_4 showed a broad peak around 3400 cm^{-1} and a sharp peak at 1650 cm^{-1}, which corresponds to the –OH stretching and bending vibrations of surface anchored H_2O molecules, respectively.[17] The

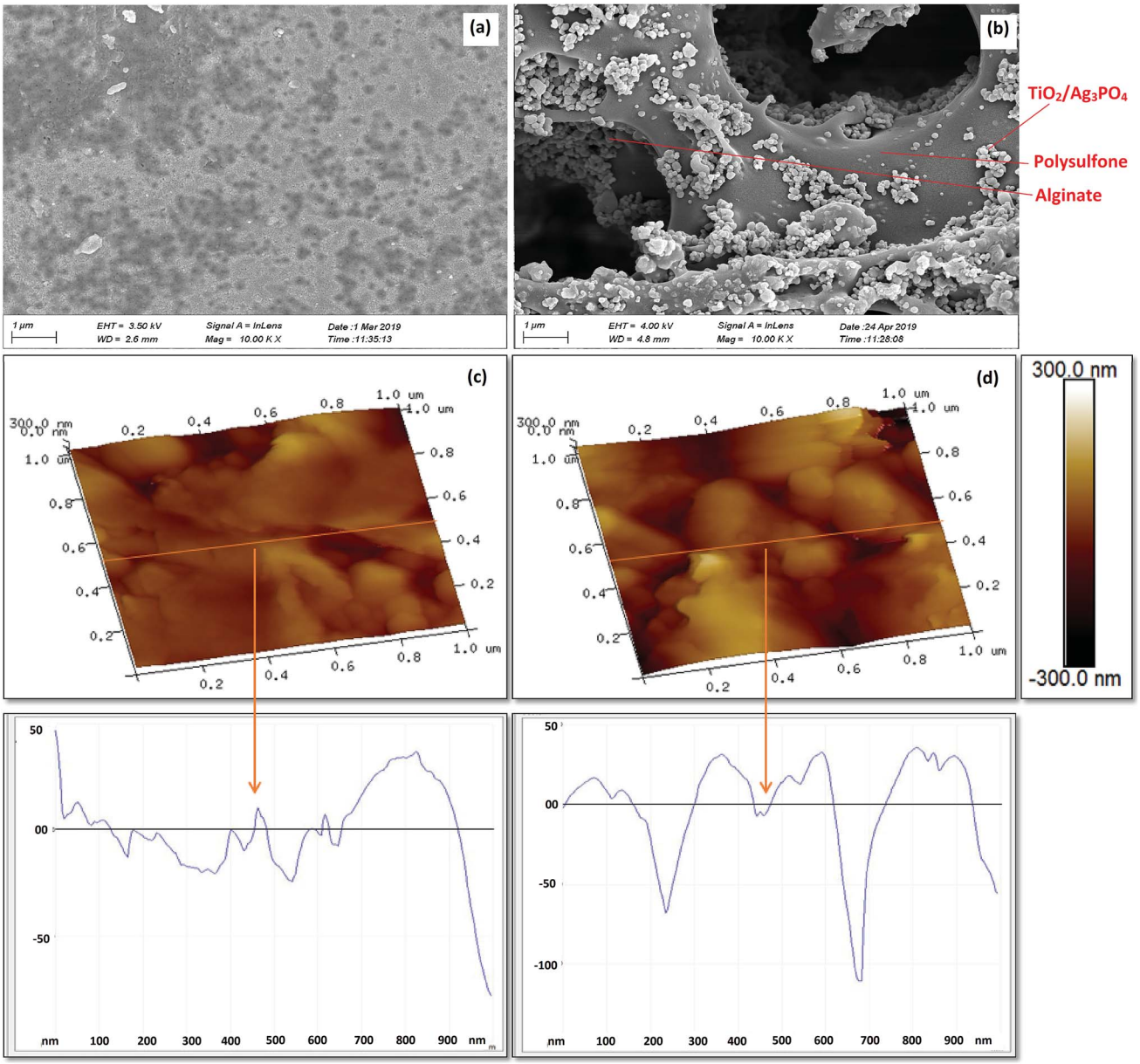

Fig. 3 SEM images of PSF/Alg beads (a) and photocatalytic beads (b), and 3D surface profilometry of PSF/Alg beads (c) and photocatalytic (PATAg) beads (d).

peaks at 560, 1013, and 1388 cm^{-1} are attributed to the O=P–O bending vibration, asymmetric stretching vibrations of P–O–P rings, and P=O stretching vibration, respectively. The peak for stretching vibrations of P–O–P has shifted to 986 cm^{-1} in TiO_2/Ag_3PO_4 composite, indicating strong interaction within the composite, which ensures the stability of the composite material.

Fig. 1b also shows the characteristic absorption bands of polymers (Table 1). All the PSF peaks are visible in both PSF/Alg and PATAg composite beads. However, the absorption peaks of alginate were masked by PSF and TiO_2 owing to their higher concentrations. No additional peaks appeared in the PATAg composite beads, which indicates that the entrapped TiO_2/Ag_3PO_4 nanoparticles did not disrupt the polymer structure. Meanwhile, the wide peak around 3450 cm^{-1}, corresponding to

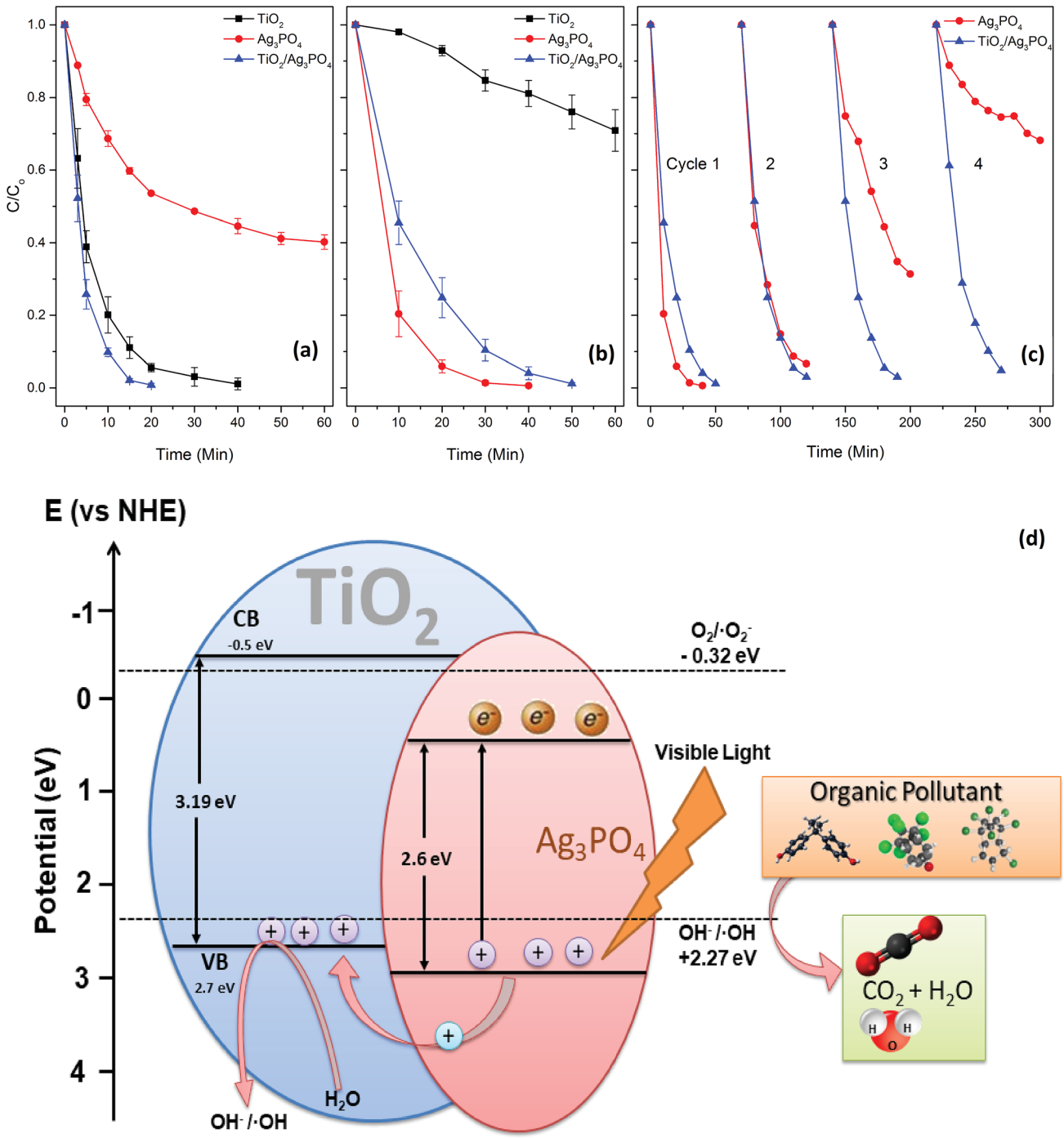

Fig. 4 Photocatalytic degradation of MB over various powdered photocatalysts under (a) UV and (b) visible light; (c) repeated use of powdered TiO_2 and TiO_2/Ag_3PO_4 under visible light; (d) schematic diagram showing the mechanism of photocatalytic degradation. ($[MB]_0$ = 3.2 mg L^{-1}; pH = 7; reaction volume = 0.8 L; catalyst dose (powdered) = 50 mg L^{-1}).

the stretching vibration of hydroxyl groups, became weaker in PATAg beads, indicating the strong interaction between these groups and TiO_2/Ag_3PO_4.

Nitrogen adsorption–desorption isotherm is a widely used technique to investigate porous structure and BET surface area of a material. As shown in Fig. 2a, the as-prepared photocatalysts exhibited type IV isotherms according to BDDT (Brunauer–Deming–Deming–Teller) classification with hysteresis loops at the relative pressure from 0.5 to 0.9 for TiO_2 and TiO_2/Ag_3PO_4 and from 0.8 to 1.0 for Ag_3PO_4, which indicates the mesoporous structure of the catalysts.[2] The corresponding pore sizes of TiO_2 and Ag_3PO_4 overlapped from 30–60 nm, while a peak at approximately 10 nm was only shown for TiO_2 (Fig. 2b and S2†). The TiO_2/Ag_3PO_4 composites displayed a different pore size distribution with a dominant peak around 10 nm. The BET specific surface area of TiO_2/Ag_3PO_4 (65.2 $m^2\ g^{-1}$) was higher than TiO_2 (49.5 $m^2\ g^{-1}$) and Ag_3PO_4 (7.9 $m^2\ g^{-1}$). The least surface area of Ag_3PO_4 can be attributed to the greatest pore size of the Ag_3PO_4, as observed in a previous report[2] and discussed in a recent review.[18] With the immobilization of TiO_2/Ag_3PO_4 composite in the PATAg beads, the pores at approximately 10 nm vanished and pores from 30–90 nm of the PSF/Alg

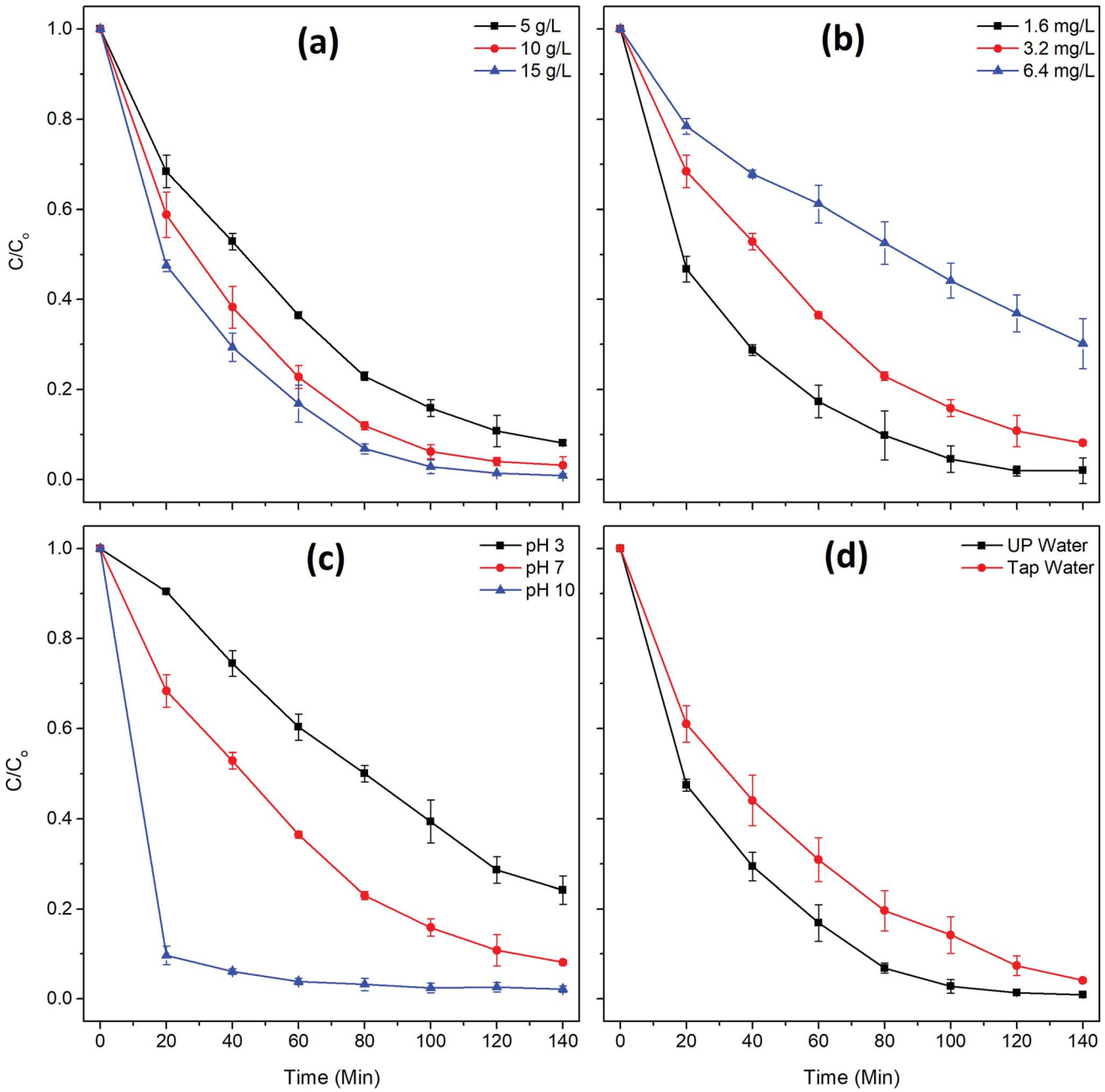

Fig. 5 Effects of various treatments on photocatalytic degradation of MB using photocatalytic beads under visible light irradiation; (a) catalyst dose; (b) initial dye concentration; (c) pH; and (d) background ions.

Table 2 Comparison of rate constants for MB (3.2 mg L^{-1}), DCF (20 mg L^{-1}), TCS (20 mg L^{-1}) degradation and *Pseudomonas fluorescens* ($\sim 10^6$ CFU mL^{-1}) inactivation using powdered and immobilized photocatalysts

		Pseudo-1st order rate constant k (min^{-1})			
		Dose (powder): 50 mg L^{-1}			
Solution	Light source	TiO_2	Ag_3PO_4	TiO_2/Ag_3PO_4	PATAg beads
MB	UV	0.1218	0.0191	0.2457	
	Visible	0.0054	0.1344	0.0826	0.0344 (15 g L^{-1})
					0.0262 (10 g L^{-1})
					0.0182 (5 g L^{-1})
DCF	Visible			0.0813	0.0184 (10 g L^{-1})
TCS	Visible			0.3003	0.0520 (10 g L^{-1})
Pseudomonas fluorescens	Visible				0.0274 (10 g L^{-1})

composite dominated (Fig. 2c, d and S2†). Meanwhile, the addition of the TiO_2/Ag_3PO_4 composite doubled the BET surface area of the PSF/Alg beads (2.7 $m^2 g^{-1}$ to 5.4 $m^2 g^{-1}$).

The UV-vis absorption spectra of TiO_2, Ag_3PO_4 and TiO_2/Ag_3PO_4 composite are shown in Fig. S1a† and corresponding bandgap energies were calculated using Tauc plot (Fig. S1b†). Ag_3PO_4 can effectively absorb visible light less than 700 nm, while pure TiO_2 can only absorb light less than 380 nm. The TiO_2/Ag_3PO_4 composite extended the light absorbance of TiO_2 to 550 nm, suggesting that the composite can harvest much more visible light than the pure TiO_2 and thus suitable for visible light photocatalytic reactions (Fig. S1a†). The emission spectra of UV and visible (LED) light sources used in this study were examined and shown in Fig. S1c.† UV lamp emits at 254 nm, whereas the LED lamp emits in a broad spectrum from 400 to 700 nm with two peaks at *ca.* 450 and 540 nm. These peaks coincide with the absorbance spectrum of TiO_2/Ag_3PO_4 composite, suggesting suitable excitation with the light sources.

The SEM analyses show a very smooth outer surface of PSF/Alg beads (Fig. 3a) contrary to the PATAg beads (Fig. 3b). Most importantly, macropores (4 to 8 μm) appeared uniformly throughout the surface of PATAg beads. It was also observed that TiO_2/Ag_3PO_4 formed randomly scattered agglomerates on the surface and inside the pores. All of these resulted in significantly higher surface roughness of the PATAg beads ($R_a = 45 \pm 9$) compared to PSF/Alg beads ($R_a = 20 \pm 5$), as indicated by the scanning probe microscopy (SMP) analysis (Fig. 3c and d). These results suggest that the addition of TiO_2/Ag_3PO_4 significantly improved the advanced pore structure of the photocatalytic beads.

Thermo-Gravimetric Analysis (TGA) was performed to characterize the temperature-induced degradation of different beads (Fig. S3†). The profile of the PSF/Alg beads showed a continuous weight loss from 100–800 °C, while the PSF beads were stable at a temperature of less than 450 °C and started decomposition at higher temperatures (~500 °C). The addition of TiO_2/Ag_3PO_4 composite to the PSF/Alg beads significantly reduced the weight loss rate at a temperature below 450 °C. The prominent decomposition of PATAg beads was observed at the higher temperature (~500 °C). This improvement in thermal stability can be ascribed to the dispersion of the naturally thermally stable TiO_2/Ag_3PO_4 composite in the PSF/Alg matrix, which also indicates favorable compatibility between TiO_2/Ag_3PO_4 and PSF/Alg matrix.[19] Heat-treatment significantly altered the size and shape of the beads (Fig. S4†). However, the PATAg beads suffered a minimum loss in size and retained their shape, which can be attributed to the strong interaction between alginate and TiO_2 nanoparticles.

Alginate beads have been previously reported for the immobilization of TiO_2 and subsequent removal of different organic dyes.[20,21] However, the alginate beads are relatively soft, which can be easily damaged during real application. The use of PSF as the backbone of the immobilization material has significantly improved the durability and mechanical stability of the prepared PATAg beads. Moreover, PSF shaped the macrovoids, while Alg contributed to the formation of micropores inside the beads. This unique sponge-like structure with interconnected macrovoids and micropores would greatly facilitate the adsorption and photocatalytic capacity of the beads.

3.2. Photocatalytic degradation of MB by powdered photocatalysts

The as-prepared powdered photocatalysts were employed to degrade MB under both UV and visible light irradiation in the annular photoreactor. Under UV irradiation, the photocatalytic activity is in the order of TiO_2/Ag_3PO_4 > TiO_2 ≫ Ag_3PO_4 (Fig. 4a), while it is Ag_3PO_4 > TiO_2/Ag_3PO_4 ≫ TiO_2 under visible light irradiation (Fig. 4b). The photocatalytic activity of materials under UV irradiation can be explained based on the fact that TiO_2 has a more negative potential of the conduction band (CB) and valence band (VB) than that of Ag_3PO_4; therefore, the photo-induced holes in the VB of Ag_3PO_4 can transfer to the VB of TiO_2 (Fig. 4d), thus contributing to efficient separation of electron–hole pairs.[2] The lower band gap energy of the TiO_2/Ag_3PO_4 composite (3.12 eV) than that of TiO_2 (3.19 eV) also plays and important role in deciding photocatalytic efficiency (Fig. S1b†). The pure TiO_2 photocatalyst showed a very low visible-light photocatalytic activity for MB degradation (k = 0.0054 min^{-1}). This is attributed to the weak visible light absorption of TiO_2. The pronounced enhancement of the photocatalytic activity of TiO_2/Ag_3PO_4 is attributable to the

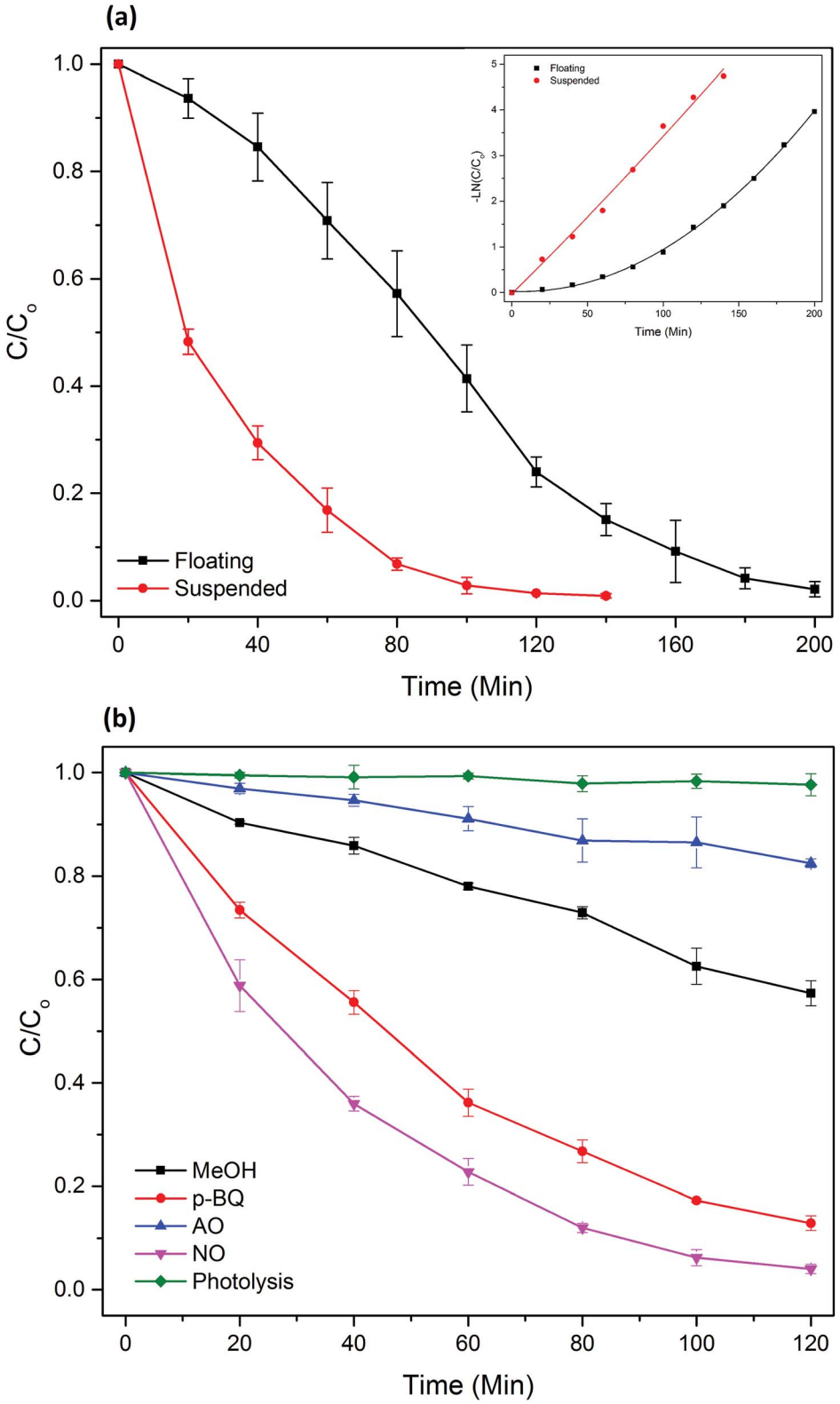

Fig. 6 Photocatalytic degradation of MB (3.2 mg L^{-1}) with suspended (15 g L^{-1}) and floating (15 g L^{-1}) form of photocatalyst beads under visible light irradiation (a) [inset: $-\ln(C/C_o)$ *vs.* time]; effect of ROS scavengers during MB degradation by PATAg beads (b). (MeOH – methanol; *p*-BQ – 1,4-benzoquinone; AO – ammonium oxalate; NO – without scavenger; error bars represent standard deviation of the mean, $n = 2$).

heterojunction of Ag_3PO_4 and TiO_2. The enhancement effect of Ag_3PO_4 is a function of the weight percent (wt%) of Ag_3PO_4 to TiO_2. It is noteworthy that the rate of MB degradation quickly increases to 0.1576 min^{-1} when 10% (weight percentage) of Ag_3PO_4 is loaded to the TiO_2. Ag_3PO_4 plays an important role in the photocatalytic activity of the Ag_3PO_4/TiO_2 composite

(Fig. S5†). Whereas, the pure silver phosphate showed higher photocatalytic degradation of MB than that of TiO_2 and TiO_2/Ag_3PO_4 composite. This is mainly due to the quantity of silver phosphate, which is highly diluted in the TiO_2/Ag_3PO_4 composite, and titania – a larger constituent – is photoactive only under UV radiation. Thus, the amount of Ag_3PO_4 in TiO_2/Ag_3PO_4 composite determines the photocatalytic activities under visible light irradiation. The lower photocatalytic activity of TiO_2/Ag_3PO_4 compared to Ag_3PO_4 under visible light is probably due to the much less (10%) content of Ag_3PO_4 in the composite.

These photocatalytic beads and powdered photocatalyst could be easily regenerated by stirring in an aqueous solution of H_2O_2 (0.5%) for 5 minutes (Fig. S6†). Repeated regeneration and visible light illumination (Fig. 4c) revealed that the TiO_2/Ag_3PO_4 composite retained its photocatalytic activity for 4 cycles. Simultaneously, Ag_3PO_4 quickly lost its photoactivity and achieved only 35% MB degradation during the fourth cycle. The effect of catalyst dose on MB degradation was also investigated. The MB degradation rate increased with the increase in the photocatalyst dose until 0.8 mg mL^{-1}, where the highest degradation rate (k = 0.124 min^{-1}) was achieved. In contrast, a further increase in the photocatalyst dose slightly declined the MB degradation rate (Fig. S7†). Too much photocatalyst dose made the MB solution turbid and hindered light penetration, resulting in a declined photoactivity.

3.3. Adsorption and photocatalytic degradation of MB by immobilized photocatalysts

3.3.1. Adsorption of MB over prepared beads. The adsorption capacity of PSF, PSF/Alg, and PATAg beads was evaluated firstly, as photocatalytic activity of these beads largely depends on the ability of the catalysts to adsorb target pollutants.[22] As expected, addition of alginate in the PSF matrix significantly enhanced the adsorption capacity of the beads (Fig. S8†), which was further improved with the addition of TiO_2/Ag_3PO_4. After 6 h, the maximum MB adsorption achieved by the beads was 28, 45, and 59% for PSF, PSF/Alg, and PATAg beads, respectively.

3.3.2. Photocatalytic degradation of MB with suspended PATAg beads. The effect of photocatalytic beads dose (5, 10, 15 g L^{-1}) on MB degradation efficiency was determined in the concurrent adsorption-photodegradation process. Under the tested condition, consecutive increments in MB degradation efficiency were observed with the increase in the beads dose (Fig. 5a), and the degradation rate constant (k) was almost linearly increased, *i.e.*, 0.0182, 0.0262 and 0.0344 min^{-1} for 5, 10 and 15 g L^{-1}, respectively (Table 2).

Three different initial dye concentrations (1.6, 3.2, 6.4 mg L^{-1}) were tested at a fixed-dose (5 g L^{-1}) of the bead photocatalyst (Fig. 5b). The diluted dye solution (1.6 mg L^{-1}) was degraded much faster (k = 0.0321 min^{-1}) compared to the concentrated (6.4 mg L^{-1}) dye solution (k = 0.0084 min^{-1}). Photocatalytic degradation of dye molecules primarily depends on the formation of reactive species on the surface of catalyst under light irradiation and their reaction with the adsorbed dye molecules. Therefore, the MB degradation rate of the tests was catalyst limited. Nevertheless, at a higher initial dye concentration, the photocatalyst may be shielded by dye molecules, thus decreasing the number of photons reaching the catalyst surface.[23]

The TiO_2/Ag_3PO_4 composite can have different surface charges, bearing with positive charges under acidic conditions and negative charges under alkaline conditions. This can be explained based on the point of zero charge (pH 6.3) of TiO_2/Ag_3PO_4. On the other hand, MB is cationic in aqueous solution.[24] Therefore, the alkaline conditions are more favorable for MB adsorption due to the electrostatic attraction; on the contrary, degradation of MB decreases in acidic conditions because of the coulombic repulsion. The results in Fig. 5c show the highest MB degradation efficiency at pH 10 and the lowest at pH 3, which corresponds well with the theory. It should be noted that the interaction of TiO_2/Ag_3PO_4 composite with the PSF/Alg matrix also affects the surface properties of catalysts, and thus influencing the adsorption and degradation of pollutants on catalysts. The interfering effect of other ions (Table S1†) on MB degradation was evaluated with tap water as the working solution (Fig. 5d). The degradation rate was higher in UP water (k = 0.0344 min^{-1}) compared to tap water (k = 0.0215 min^{-1}), which could be explained by the competition of other ions present in the tap water for active sites.[25]

3.3.3. Photocatalytic degradation of MB with buoyant PATAg beads. Buoyant photocatalytic beads are very attractive for environmental applications, as they are localized at the air/water interface, thus receiving the highest solar/visible light intensity. The PATAg beads can be switched to either suspended or floating form by a simple drying or wetting procedure. To compare the photocatalytic activity of the two forms, we used an equal number of photocatalytic beads (wet weight ~15 g L^{-1}) in two photoreactors with a 0.8 L working volume to treat 3.2 mg L^{-1} MB solution. The results show that in suspended form, complete degradation of MB was achieved within 120 minutes. However, this was extended to 200 minutes in floating

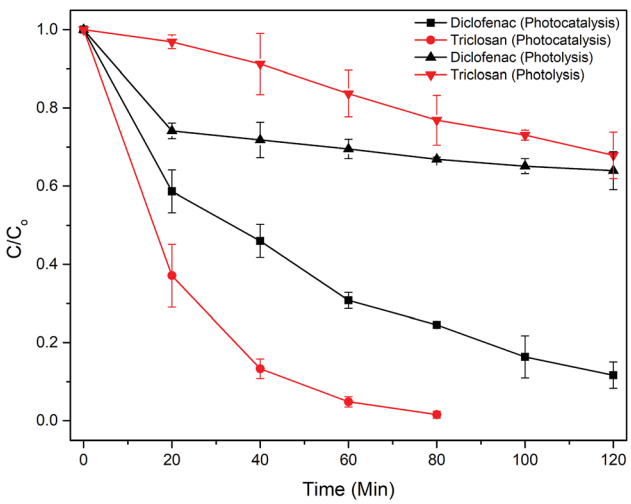

Fig. 7 Photocatalytic degradation of pharmaceutical compounds by the PATAg beads under visible light (initial drug concentration = 20 mg L^{-1}; beads loading = 10 g L^{-1}; reaction volume 0.8 L).

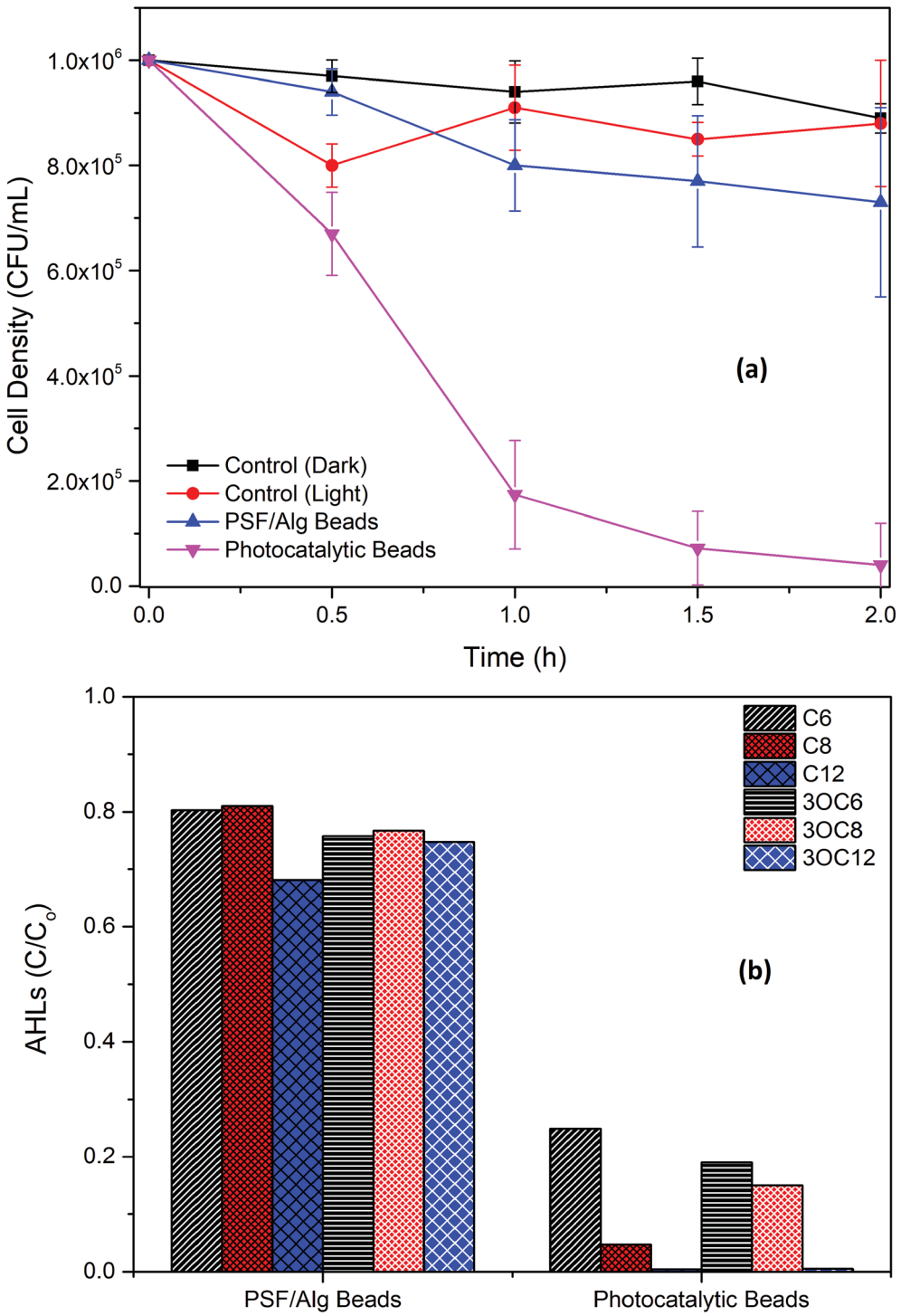

Fig. 8 Photocatalytic inactivation of bacterial strain (a); and photocatalytic degradation of AHLs (b).

form (Fig. 6a). The lower photodegradation in the floating form could be explained by its less quantum yield, lower oxygen mass transfer, and MB mass transfer limitation.[3] Even though the photoactivity of the as-prepared PATAg beads in floating form was lower than that in suspended form, it is still very promising to utilize them under visible light and constrained conditions, *e.g.*, no stirring and aeration, with almost no energy input. The floating PATAg beads can be reused for several consecutive times without any significant decrease in photocatalytic activity. The form of these beads can also be inter-switched multiple times without any significant deterioration to the beads.

3.3.4. Mechanism of photocatalytic degradation of MB. AO, MeOH, and *p*-BQ, the typical h^+, $^{\bullet}OH$ and $O_2^{\bullet-}$ scavengers,[26,27] respectively, were used to determine the role of ROS

during MB degradation under visible light by PATAg beads. The degradation rate constant of MB (Fig. 6b) was reduced by 37%, 81% and 93% in presence of *p*-BQ ($k = 0.017\ min^{-1}$), MeOH ($k = 0.005\ min^{-1}$) and AO ($k = 0.002\ min^{-1}$), respectively, as compared to without a scavenger ($k = 0.027\ min^{-1}$), suggesting the primary role of h^+ and $^{\bullet}OH$ radicals in the MB photodegradation among all ROS. The $^{\bullet}OH$ radicals can attack the C–S^+=C functional group in MB, which is the initial step of MB degradation.[28]

The primary route of $^{\bullet}OH$ formation is well reported as the oxidation of OH^- or water at the TiO_2 surface through the highly oxidizing h^+;[26,29] hence, scavenging of h^+ almost completely stopped $^{\bullet}OH$ formation, and thus MB photodegradation. Importantly, none of the ROS completely stopped the MB degradation, which implies that not a single ROS is solely responsible for the process. Additionally, MB is not prone to photodegradation under visible light ($k = 0.0002\ min^{-1}$).

Comparing with the ROS scavenging experiments of photocatalytic TiO_2 beads under UV, where quenching the h^+ with the addition of AO only resulted in a 33% reduction in the reaction rate constant, the h^+ radicals played a significantly greater role in MB degradation by the TiO_2/Ag_3PO_4 beads. This observation indicates that, under visible light, the ROS are generated primarily through valence band holes on TiO_2/Ag_3PO_4 composite, while a lot of ROS were generated through conduction band electrons on TiO_2 nanoparticles. Therefore, these excited electrons were mostly trapped by Ag_3PO_4, suggesting the effective heterojunction between TiO_2 and Ag_3PO_4.[7,8]

3.4. Photocatalytic degradation of pharmaceuticals

The Fig. 7 shows that triclosan was completely degraded ($k = 0.052\ min^{-1}$) within 80 min of photocatalysis, while it took 120 min for diclofenac ($k = 0.018\ min^{-1}$). Powdered TiO_2/Ag_3PO_4 composite was also tested for drugs degradation, and showed higher rate constants compared to immobilized photocatalyst (Fig. S9†) due to larger surface area and more efficient utilization of light. However, powdered photocatalysts are difficult to recycle and reuse. New peaks at 235, 256, 279, 289 nm and a broad peak from 320 to 340 nm emerged in the UV-vis scan of diclofenac (Fig. S10†) after 5 minutes of reaction, indicating the appearance of intermediate compounds. As indicated by the peaks of 275–280 nm in the UV spectra, the aromatic intermediates were probably more resistant to photocatalysis than the diclofenac residual, as reported earlier.[30] Photocatalytic degradation of diclofenac using the ZnO–WO_3 catalysts, prepared with different molar ratios, was carried out by Muguntan *et al.*,[31] and an apparent rate constant for first-order kinetics of $\sim 0.0131\ min^{-1}$ was reported. Chen *et al.*,[32] reported a similar degradation rate constant of $0.013\ min^{-1}$ for diclofenac with WS_2 nanosheets. These rate constants are significantly less than the present study despite a higher visible light intensity.

As emerging contaminants, triclosan and diclofenac have attracted a lot of interest due to their adverse impacts on human health and environments. Especially, diclofenac has been listed on the watch list of water contaminants by the EU Water Framework Directive (Decision 2015/495) since 2015. The environmentally relative concentrations of these two PhACs are typically in the range of $<1\ \mu g\ L^{-1}$; hence, photocatalysis is a promising technology to polish the water contaminated with trace amounts of PhACs.

3.5. Photocatalytic disinfection and quorum quenching (AHLs degradation)

Bacterial disinfection was carried out in Petri dishes with the bacterial strain (*Pseudomonas fluorescens*). After exposure to visible light for 90 min, the PATAg beads effectively disinfected the strain, while the controls (light and dark) and PSF/Alg beads presented negligible inactivation (Fig. 8a). As leaching of Ti and Ag ions from the PATAg beads was not observed (Table S2†), this bacterial inactivation was majorly attributed to the ROS generated under visible light. This highly effective disinfection capability of PATAg beads can be utilized as an alternative to UV disinfection for posttreatment of effluents in decentralized wastewater treatment facilities.

Prominent AHL compounds were also tested for their degradation under visible light using PATAg beads in floating form (Fig. 8b). It can be seen that C6-, 3OC6-, and 3OC6-AHLs were removed over 80% after 90 min, while C8-AHL was removed over 95%, and C12- and 3OC12-AHLs were almost completed removed. It is also noticed that the adsorption of all AHLs to the PSF/Alg matrix was less than 25–30%. The AHL degradation efficiencies of these PATAg beads were much higher than that of a typic QQ strain (data not shown), which indicates that the photocatalytic QQ with PATAg beads can be used as a very efficient technology for biofilm control.

4. Conclusions

In this study, we have successfully prepared TiO_2/Ag_3PO_4 nanoparticles and immobilized them onto the polysulfone–alginate matrix to form visible light-active photocatalytic polymer beads, termed as PATAg beads. The major conclusions are as follows.

(1) The addition of Ag_3PO_4 does not have any negative impacts on the sponge-like structure of the photocatalytic polymer beads. The macrovoids of 30–90 nm dominate the beads, and provide a BET surface area of $5.4\ m^2\ g^{-1}$. The synergistic interactions between the catalysts and the immobilization material provide exceptional thermal stability of the beads.

(2) The PATAg beads show a very high visible light photocatalytic activity towards MB, TCS and DCF in the suspended form with a 100% removal time of 120, 80 and 120 min, respectively. The $^{\bullet}OH$ radicals are determined to be the primary ROS responsible for the photocatalytic reactions.

(3) The PATAg beads can be easily switched between the suspended and the buoyant form. The PATAg beads remained its high visible light photocatalytic activity in the buoyant form, removing MB completely within 200 minutes under stagnant condition.

(4) The PATAg beads can be effectively regenerated by H_2O_2 treatment and used for multiple cycles without any significant loss in photoactivity.

With these features, it is believed that this hybrid system is pragmatic for applications in engineered and natural (waste) water treatment systems at larger scales.

Conflicts of interest

There are no conflicts to declare.

Acknowledgements

This research was jointly supported by the Key-Area Research and Development Program of Guangdong Province, China (No. 2019B110205003), the National Natural Science Foundation of China (No. 51750110514), the Science and Technology Planning Project of Guangdong Province, China (No. 809130915092), and Shantou University Scientific Research Foundation for Talents (No. NTF16015).

References

1 A. Chenchana, A. Nemamcha, H. Moumeni, J. M. Doña Rodríguez, J. Araña, J. A. Navío, O. González Díaz and E. Pulido Melián, Photodegradation of 2,4-dichlorophenoxyacetic acid over TiO_2 (B)/anatase nanobelts and Au-TiO_2 (B)/anatase nanobelts, *Appl. Surf. Sci.*, 2019, **467–468**, 1076–1087.

2 Y. Liu, W. Wang, M. Si, Y. Yu and H. Zhang, (Yb^{3+},Er^{3+}) co-doped TiO_2/Ag_3PO_4 hybrid photocatalyst with enhanced activity for photodegradation of phenol, *Appl. Surf. Sci.*, 2019, **463**, 159–168.

3 Z. Xing, J. Zhang, J. Cui, J. Yin, T. Zhao, J. Kuang, Z. Xiu, N. Wan and W. Zhou, Recent advances in floating TiO_2-based photocatalysts for environmental application, *Appl. Catal., B*, 2018, **225**, 452–467.

4 K. Baďurová, O. Monfort, L. Satrapinskyy, E. Dworniczek, G. Gościniak and G. Plesch, Photocatalytic activity of Ag_3PO_4 and some of its composites under non-filtered and UV-filtered solar-like radiation, *Ceram. Int.*, 2017, **43**, 3706–3712.

5 T. Cai, Y. Liu, L. Wang, S. Zhang, Y. Zeng, J. Yuan, J. Ma, W. Dong, C. Liu and S. Luo, Silver phosphate-based Z-Scheme photocatalytic system with superior sunlight photocatalytic activities and anti-photocorrosion performance, *Appl. Catal., B*, 2017, **208**, 1–13.

6 Y. Bi, S. Ouyang, N. Umezawa, J. Cao and J. Ye, Facet Effect of Single-Crystalline Ag_3PO_4 Sub-microcrystals on Photocatalytic Properties, *J. Am. Chem. Soc.*, 2011, **133**, 6490–6492.

7 F. M. Zhao, L. Pan, S. Wang, Q. Deng, J. J. Zou, L. Wang and X. Zhang, Ag_3PO_4/TiO_2 composite for efficient photodegradation of organic pollutants under visible light, *Appl. Surf. Sci.*, 2014, **317**, 833–838.

8 L. Yang, W. Duan, H. Jiang, S. Luo and Y. Luo, Mesoporous TiO_2@Ag_3PO_4 photocatalyst with high adsorbility and enhanced photocatalytic activity under visible light, *Mater. Res. Bull.*, 2015, **70**, 129–136.

9 C. Chi, J. Pan, M. You, Z. Dong, W. Zhao, C. Song, Y. Zheng and C. Li, The porous TiO_2 nanotubes/Ag_3PO_4 heterojunction for enhancing sunlight photocatalytic activity, *J. Phys. Chem. Solids*, 2018, **114**, 173–178.

10 B. Srikanth, R. Goutham, R. Badri Narayan, A. Ramprasath, K. P. Gopinath and A. R. Sankaranarayanan, Recent advancements in supporting materials for immobilised photocatalytic applications in waste water treatment, *J. Environ. Manage.*, 2017, **200**, 60–78.

11 Z. Shi, Y. Zhang, G. Duoerkun, W. Cao, T. Liu, L. Zhang, J. Liu, M. Li and Z. Chen, Fabrication of MoS_2/BiOBr heterojunctions on carbon fibers as a weaveable photocatalyst for tetracycline hydrochloride degradation and Cr(VI) reduction under visible light, *Environ. Sci.: Nano*, 2020, **7**, 2708–2722.

12 I. Dalponte, B. C. de Sousa, A. L. Mathias and R. M. M. Jorge, Formulation and optimization of a novel TiO_2/calcium alginate floating photocatalyst, *Int. J. Biol. Macromol.*, 2019, **137**, 992–1001.

13 M. J. Martín de Vidales, A. Nieto-Márquez, D. Morcuende, E. Atanes, F. Blaya, E. Soriano and F. Fernández-Martínez, 3D printed floating photocatalysts for wastewater treatment, *Catal. Today*, 2019, **328**, 157–163.

14 M. Sboui, M. F. Nsib, A. Rayes, M. Swaminathan and A. Houas, TiO_2–PANI/Cork composite: a new floating photocatalyst for the treatment of organic pollutants under sunlight irradiation, *J. Environ. Sci.*, 2017, **60**, 3–13.

15 C. Zhou, Y. Zhao, J. Cao, H. Lin and S. Chen, Partial oxidation controlled activity regeneration of used Ag_3PO_4 photocatalyst *via* removing the *in situ* surface metallic silver, *Appl. Surf. Sci.*, 2015, **351**, 33–39.

16 X. Zhang, K. Lee, H. Yu, N. Mameda and K.-H. Choo, Photolytic quorum quenching: a new anti-biofouling strategy for membrane bioreactors, *Chem. Eng. J.*, 2019, **378**, 122235.

17 L. Liu, Y. Qi, J. Lu, S. Lin, W. An, Y. Liang and W. Cui, A stable Ag_3PO_4@g-C_3N_4 hybrid core@shell composite with enhanced visible light photocatalytic degradation, *Appl. Catal., B*, 2016, **183**, 133–141.

18 M. Al Kausor, S. Sen Gupta and D. Chakrabortty, Ag_3PO_4-based nanocomposites and their applications in photodegradation of toxic organic dye contaminated wastewater: review on material design to performance enhancement, *J. Saudi Chem. Soc.*, 2020, **24**, 20–41.

19 A. T. Kuvarega, N. Khumalo, D. Dlamini and B. B. Mamba, Polysulfone/N,Pd co-doped TiO_2 composite membranes for photocatalytic dye degradation, *Sep. Purif. Technol.*, 2018, **191**, 122–133.

20 R. Aravindhan, N. N. Fathima, J. R. Rao and B. U. Nair, Equilibrium and thermodynamic studies on the removal of basic black dye using calcium alginate beads, *Colloids Surf., A*, 2007, **299**, 232–238.

21 V. Rocher, J.-M. Siaugue, V. Cabuil and A. Bee, Removal of organic dyes by magnetic alginate beads, *Water Res.*, 2008, **42**, 1290–1298.

22 N. M. Mahmoodi, B. Hayati, M. Arami and H. Bahrami, Preparation, characterization and dye adsorption properties of biocompatible composite (alginate/titania nanoparticle), *Desalination*, 2011, **275**, 93–101.

23 M. Thomas, T. S. Natarajan, M. U. D. Sheikh, M. Bano and F. Khan, Self-organized graphene oxide and TiO_2 nanoparticles incorporated alginate/carboxymethyl cellulose nanocomposites with efficient photocatalytic activity under direct sunlight, *J. Photochem. Photobiol., A*, 2017, **346**, 113–125.

24 C. Zhu, L. Wang, L. Kong, X. Yang, L. Wang, S. Zheng, F. Chen, F. MaiZhi and H. Zong, Photocatalytic degradation of AZO dyes by supported TiO_2 + UV in aqueous solution, *Chemosphere*, 2000, **41**, 303–309.

25 J. Gjipalaj and I. Alessandri, Easy recovery, mechanical stability, enhanced adsorption capacity and recyclability of alginate-based TiO_2 macrobead photocatalysts for water treatment, *J. Environ. Chem. Eng.*, 2017, **5**, 1763–1770.

26 T. Jedsukontorn, T. Ueno, N. Saito and M. Hunsom, Mechanistic aspect based on the role of reactive oxidizing species (ROS) in macroscopic level on the glycerol photooxidation over defected and defected-free TiO_2, *J. Photochem. Photobiol., A*, 2018, **367**, 270–281.

27 M. Pelaez, P. Falaras, V. Likodimos, K. O'Shea, A. A. de la Cruz, P. S. M. Dunlop, J. A. Byrne and D. D. Dionysiou, Use of selected scavengers for the determination of NF-TiO_2 reactive oxygen species during the degradation of microcystin-LR under visible light irradiation, *J. Mol. Catal. A: Chem.*, 2016, **425**, 183–189.

28 A. Houas, H. Lachheb, M. Ksibi, E. Elaloui, C. Guillard and J. M. Herrmann, Photocatalytic degradation pathway of methylene blue in water, *Appl. Catal., B*, 2001, **31**, 145–157.

29 J. Trawiński and R. Skibiński, Rapid degradation of clozapine by heterogeneous photocatalysis. Comparison with direct photolysis, kinetics, identification of transformation products and scavenger study, *Sci. Total Environ.*, 2019, **665**, 557–567.

30 L. Rizzo, S. Meric, D. Kassinos, M. Guida, F. Russo and V. Belgiorno, Degradation of diclofenac by TiO_2 photocatalysis: UV absorbance kinetics and process evaluation through a set of toxicity bioassays, *Water Res.*, 2009, **43**, 979–988.

31 E. Mugunthan, M. B. Saidutta and P. E. Jagadeeshbabu, Photocatalytic activity of ZnO-WO_3 for diclofenac degradation under visible light irradiation, *J. Photochem. Photobiol., A*, 2019, **383**, 111993.

32 Z. Chen, S. He, M. Zhu and C. Wei, The effect of peroxymonosulfate in WS_2 nanosheets for the removal of diclofenac: Information exposure and degradation pathway, *Chemosphere*, 2020, **245**, 125678.

